Schizophrenia Research 235 (2021) 17–28

Contents lists available at ScienceDirect

Schizophrenia Research

journal homepage: www.elsevier.com/locate/schres

Neuroplasticity and inflammatory alterations in the nucleus accumbens are corrected after risperidone treatment in a schizophrenia-related developmental model in rats

Hiram Tendilla-Beltrán [a,b,c,d], Heriberto Coatl-Cuaya [a,b], Silvia Meneses-Prado [a], Ruben Antonio Vázquez-Roque [a], Eduardo Brambila [e], Miguel Tapia-Rodríguez [f], David Martín-Hernández [g], Linda Garcés-Ramírez [b], José L.M. Madrigal [c,d,h], Juan C. Leza [c,d,h,*], Gonzalo Flores [a,**]

[a] Instituto de Fisiología, Benemérita Universidad Autónoma de Puebla (BUAP), Puebla 72570, Mexico
[b] Escuela Nacional de Ciencias Biológicas (ENCB), Instituto Politécnico Nacional (IPN), CDMX 11340, Mexico
[c] Departamento de Farmacología y Toxicología, Facultad de Medicina, Universidad Complutense de Madrid (UCM), Madrid 28040, Spain
[d] Instituto Universitario de Investigación en Neuroquímica (IUIN), UCM, Spain
[e] Facultad de Ciencias Químicas, BUAP, Mexico
[f] Instituto de Investigaciones Biomédicas (IIBO), Universidad Nacional Autónoma de México (UNAM), CDMX 04510, Mexico
[g] Servicio de Psiquiatría del Niño y del Adolescente, Instituto de Psiquiatría y Salud Mental, Hospital General Universitario Gregorio Marañón, Facultad de Medicina, Universidad Complutense, IiSGM, CIBERSAM, Madrid, Spain
[h] Centro de Investigación Biomédica en Red de Salud Mental (CIBERSAM), Instituto de Investigación Sanitaria Hospital 12 de Octubre (Imas12), Madrid 28029, Spain

ARTICLE INFO

Keywords:
Atypical antipsychotics
Spiny projection neurons
Stereology
MAP kinases
Nrf2
Smad

ABSTRACT

Increased dopaminergic activity in the striatum underlies the neurobiology of psychotic symptoms in schizophrenia (SZ). Beyond the impaired connectivity among the limbic system, the excess of dopamine could lead to inflammation and oxidative/nitrosative stress. It has been suggested that atypical antipsychotic drugs attenuate psychosis not only due to their modulatory activity on the dopaminergic/serotonergic neurotransmission but also due to their anti-inflammatory/antioxidant effects. In such a manner, we assessed the effects of the atypical antipsychotic risperidone (RISP) on the structural neuroplasticity and biochemistry of the striatum in adult rats with neonatal ventral hippocampus lesion (NVHL), which is a developmental SZ-related model. RISP administration (0.25 mg/kg, i.p.) ameliorated the neuronal atrophy and the impairments in the morphology of the dendritic spines in the spiny projection neurons (SPNs) of the ventral striatum (*nucleus accumbens*: NAcc) in the NVHL rats. Also, RISP treatment normalized the pro-inflammatory pathways and induced the antioxidant activity of the nuclear factor (erythroid-derived 2)-like 2 (Nrf2) in this model. Our results point to the neurotrophic, anti-inflammatory, and antioxidant effects of RISP, together with its canonical antipsychotic mechanism, to enhance striatum function in animals with NVHL.

1. Introduction

Psychosis is defined as an altered mental condition in which the individual loses contact with reality. An adequate perception and understanding of the world around us is fundamental for survival (Simons et al., 2017). Thus, psychosis represents a disabling condition for people who suffer from it. Moreover, psychosis is the core symptom in schizophrenia (SZ), a mental disease which affects around 2% of the worldwide population, and whose etiology is still poorly understood. However, the neurobiology of the positive symptoms of the disease (psychotic episodes, hallucinations, delusions) has been associated with dopaminergic hyperactivity of axons from the ventral tegmental area (VTA) in the mesolimbic brain to the *nucleus accumbens* (NAcc) or ventral (also known as limbic) striatum (McCutcheon et al., 2019).

The NAcc is a basal ganglia nucleus involved in sensory-motor integration and is mainly composed of medium-sized spiny projection neurons (SPNs)

* Correspondence to: J.C. Leza, Department of Pharmacology, School of Medicine, Complutense University, 28040 Madrid, Spain.
** Correspondence to: G. Flores, Instituto de Fisiología, Benemérita Universidad Autónoma de Puebla, 14 sur 6301, 72570 Puebla, Mexico.
E-mail addresses: jcleza@med.ucm.es (J.C. Leza), gonzaloflores56@gmail.com, gonzalo.flores@correo.buap.mx (G. Flores).

https://doi.org/10.1016/j.schres.2021.07.014
Received 10 January 2021; Received in revised form 4 July 2021; Accepted 11 July 2021
Available online 20 July 2021

(McCutcheon et al., 2019). These neurons use GABA as the main neurotransmitter and receive glutamatergic inputs from the prefrontal cortex (PFC), ventral hippocampus (in rodents, anterior hippocampus in humans) also known as the limbic hippocampus, and the basolateral amygdala (O'Donnell and Grace, 1995). In SZ, there is impaired glutamatergic activity in the NAcc which through GABAergic activity disinhibits the VTA via the ventral pallidum (also a GABAergic nucleus), causing hyperactivity of the mesolimbic pathway (Sonnenschein and Grace, 2020). It has been demonstrated that dendritic spine morphology can be modulated by dopaminergic activity in the striatum of mice with increased dopaminergic striatal innervation (Aphakia mice) in a dose-dependent manner (Alberquilla et al., 2020). In this sense, mesolimbic hyperactivity can alter the synaptic surface dynamics of the SPNs in the striatum with rearrangements in the dendritic arbor and dendritic spine dynamics, as demonstrated in the NAcc of rats exposed to dopaminergic agonists (Robinson and Kolb, 1999, 1997).

The modulation of the mesolimbic activity attenuates psychotic symptoms (Abi-Dargham et al., 2000). Thus, the pharmacological target for atypical antipsychotic drugs (AADs) is the inverse agonism of dopaminergic D2 receptors in the striatum (Roberts and Strange, 2005), as well as the antagonism of 5-HT2A and agonism of 5-HT1A serotonergic receptors in the PFC (Meltzer and Massey, 2011). Also, AADs have antioxidant effects (Hendouei et al., 2018) and restore the levels of neurotrophic-related molecules in the peripheral blood of patients with SZ (Martinez-Cengotitabengoa et al., 2015).

The neonatal ventral hippocampus lesion (NVHL) in the rat is a SZ-related model which has been used to examine the antioxidant and neurotrophic effects

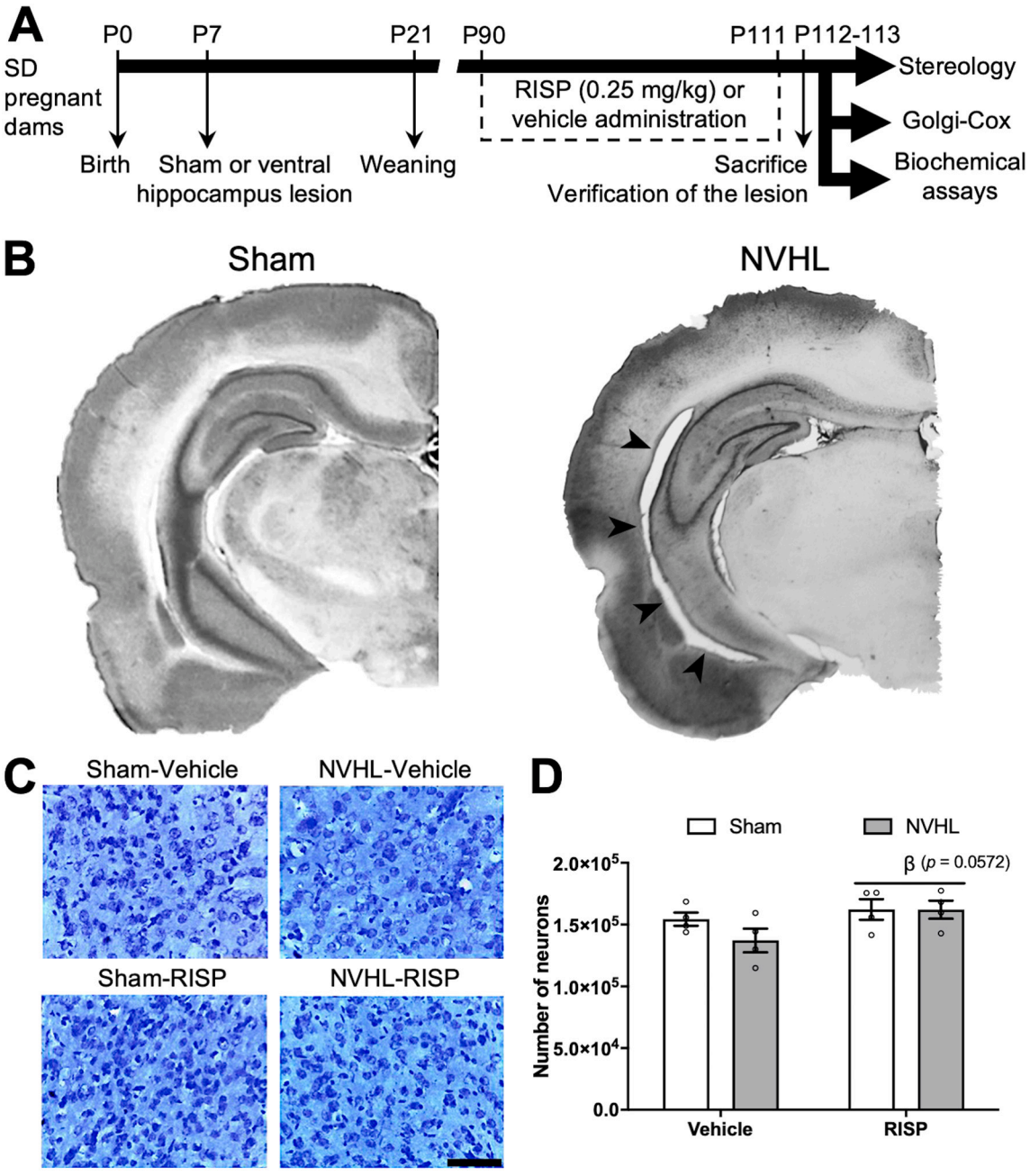

Fig. 1. A, timeline of the experimental design. B, verification of the ventral hippocampus lesion: representative photographs of sham rats with no macroscopic damage in the ventral hippocampus and NVHL rats with visible damage only in the ventral hippocampus region (indicated with the arrowheads). C, representative photomicrographs of NAcc sections stained with Nissl method of each group (scale bar = 100 μm). D, the stereological neuronal counting of NAcc neurons revealed that RISP tends to increase the number of neurons in both sham and NVHL rats (n = 4/group; two-way ANOVA, $^{\beta}$RISP main effect: p = 0.0572).

of AADs in the brain (Tendilla-Beltrán et al., 2021). The disruption of the limbic hippocampus-PFC synaptogenesis around postnatal days (P) 7-9 triggers a great number of behavioral abnormalities associated with the symptoms of the disease (Tseng et al., 2009), which are corrected after the treatment with AADs (Bringas et al., 2012; Rueter et al., 2004; Tendilla-Beltrán et al., 2019b). Also, rats with NVHL have neuronal atrophy and impaired morphology of the dendritic spines in the NAcc (Tendilla-Beltrán et al., 2019a).

A previous report of our group points out that RISP treatment at adulthood improved the contextual challenge to novel environment performance by restoring the structural neuroplasticity impairments and attenuating the oxidative/nitrosative stress (O/NS) in the PFC of rats with NVHL (Tendilla-Beltrán et al., 2019b). However, since the NAcc is the limbic-motor interface and represents the main target of the AADs because of their myriad of D2 receptors, describing the RISP effects in this brain area is necessary to understand the mechanisms by which this drug is improving behavior in rats with NVHL.

The objective of this study was to evaluate the effect of RISP on the neuronal number and structural plasticity of NAcc SPNs, and on infiammatory and antioxidant pathways in rats with NVHL, which is a neurodevelopmental SZ-related model.

2. Materials and methods

2.1. Animals

The timeline of the experimental protocol is shown in Fig. 1A. Pregnant Sprague-Dawley dams ($n = 11$) with 14–16 gestational days were obtained from our facilities (Bioterio Claude Bernard (BUAP), and Harlan). After birth (P0), at P7 only male pups ($n = 95$, 6-8 male pups per litter) were randomly assigned for either sham ($n = 44$) or NVHL surgery (n = 44), seven pups died during surgical protocol (7.3% of mortality). For details of animal housing see SI. All procedures described in the present study were performed following the BUAP Animal Care Committee (FLAG-UALVIEP-17-1) and the Guide for Care and Use of Laboratory Animals of the Mexican Council for Animal Care (Norma Oficial Mexicana NOM-062-ZOO-1999), as well as the Animal Welfare Committee of Universidad Complutense following European legislation (2010/63/EU), PROEX 008/18. Also, animal manipulation followed the ARRIVE guidelines. All efforts were made to reduce the number of animals used and minimize animal suffering in the experiments.

2.2. Surgical procedures

NVHL protocol was previously described in detail (Flores et al., 2005, 1996; Lipska et al., 1993; Monfil et al., 2018; Tendilla-Beltrán et al., 2019a; Tendilla-Beltrán et al., 2019b), and described in detail in supplementary data (SD).

2.3. RISP administration

At adulthood, animals were randomly assigned either to the vehicle or RISP group. Once a day from P90-111, animals were administered (i.p.) 0.25 mg/kg of RISP (Janssen Pharmaceutica, in 0.25% of glacial acetic acid and 0.1 M PBS) or vehicle. The RISP dose used in this study has demonstrated a behavioral enhancement in animals with NVHL (Rueter et al., 2004) and anti-infiammatory effects in the brain of rats exposed to lipopolysaccharide (MacDowell et al., 2013). After this, four experimental groups were obtained ($n = 22$/group): (1) sham-vehicle, (2) NVHL-vehicle, (3) sham-RISP, and (4) NVHL-RISP.

2.4. Tissue samples

For animals employed for the stereological neuronal count ($n = 4$/group) and neuronal morphology assessments ($n = 8$/group), their behavioral performance was assessed before and after treatment and the results were reported elsewhere (Tendilla-Beltrán et al., 2019b). Two groups of rats were used for distinct biochemical assays: one for nitrites, thiobarbituric acid reactive species (TBARS), and Western-Blot protocols ($n = 5$/group), and another for metallothionein (MT) quantification (n = 5/group). These animals were intracardially perfused with 0.9% saline solution and then the brain was removed from the skull and the striatum was excised and frozen at -80 °C until assayed.

2.5. Histological studies

2.5.1. Stereological analysis for neuronal counting

Stereological neuronal counting of the NAcc was assessed as previously reported (Tendilla-Beltrán et al., 2019b; Vázquez-Roque et al., 2012), and described in detail in SD. Optical fractionator sampling parameters are shown in Table 1.

2.5.2. Golgi–Cox stain method

To evaluate the effects of RISP on structural plasticity in the NAcc SPNs of NVHL rats, a modiffed Golgi–Cox stain method was used (Gibb and Kolb, 1998), as previously described (Flores et al., 2005; Monroy et al., 2020; Tendilla-Beltrán et al., 2016). For details see SD.

2.5.3. Neuronal reconstruction, Sholl analysis, and dendritic spines analysis

The dendritic complexity, length per branch order, and total dendritic length of 320 SPNs of the shell of the NAcc (80 per group, 10 per animal) were estimated using the Sholl analysis (Sholl, 1953). Dendritic spine number and dendritic spine morphological classiffcation was assessed as previously described (Monroy et al., 2020; Tendilla-Beltrán et al., 2019a; Tendilla-Beltrán et al., 2016). For details see SD.

2.6. Biochemical determinations

2.6.1. Western blot analysis

The relative protein levels of the molecules of interest were determined in cytosolic or nuclear extracts by Western blot as previously described (Martín-Hernández et al., 2019a, 2019b), and described in detail in SD. The primary antibodies used are listed in Table 2. Blots were imaged using the Odyssey Fc System (Li-COR Biosciences), quantified by densitometry (NIH ImageJ software), expressed in arbitrary units of optical density (O.D.), and calculated in comparison with the sham-vehicle group. For 4-HNE, p-p38, p-ERK, ERK, p-Smad-2/3, Smad 2/3, and PI3K proteins, the quantification of the double band was assessed tracing a region of interest area which contained both bands. For p-JNK and JNK proteins, the double bands detected were quantified individually and summed for each sample. β-actin (1:15000; Sigma-Aldrich, A5441; RRID: AB_476744) and GAPDH (1:5000; Sigma-Aldrich, G8795; RRID: AB_1078991) were used for loading control for cytosolic and nuclear proteins respectively. Neither β-actin nor GAPDH protein levels vary among experimental groups.

2.6.2. Nitrites

Nitrite concentration was quantiffed employing the Griess reaction (Green et al., 1982), in NAcc homogenates. For details see SD.

Table 1
Optical fractionator sampling parameters for stereological neuronal counting.

Parameter	Value
Number of sections (range)	8-10
Distance between sections	150 μm
Scan grid	800 × 800 μm
Counting frame	60 × 60 μm
Disector height	20 μm
Guard zones, upper and lower	10 μm
Average section thickness, range	36.07 μm, 30.5-41.7

Table 2
Antibodies used for Western Blot.

Antibody	Supplier/ code number	Dilution	Fraction	RRID
Rabbit polyclonal anti-Thr180/ Tyr182phospho-p38	SCBT/sc-17852-R	1:1000	Cytosolic	AB_2139810
Mouse monoclonal anti-p38α/β	SCBT/sc-7972	1:1000	Cytosolic	AB_628079
Rabbit polyclonal anti-Thr202/ Tyr204phospho-ERK	CST/8544	1:1000	Cytosolic	AB_11127856
Rabbit polyclonal anti-ERK	CST/4695	1:1000	Cytosolic	AB_390779
Rabbit polyclonal anti-Thr183/ Tyr185phospho-SAPK/JNK	CST/9251	1:1000	Cytosolic	AB_331659
Rabbit polyclonal anti-SAPK/JNK	CST/9252	1:1000	Cytosolic	AB_2250373
Rabbit monoclonal anti-phospho-Smad2 (Ser465/467)/Smad3 (Ser423/425)	CST/8828	1:1000	Cytosolic	AB_2631089
Rabbit polyclonal anti-Smad-2/3	CST/5678	1:1000	Cytosolic	AB_10693547
Rabbit monoclonal anti-Smad-4	CST/38454	1:1000	Cytosolic	AB_2728776
Rabbit polyclonal anti-PI3K	SCBT/ sc7189	1:750 (1% BSA)	Cytosolic	AB_2165408
Rabbit polyclonal anti-Ser437phospho-Akt	CST/4060	1:1000	Cytosolic	AB_2315049
Rabbit polyclonal anti-Akt	CST/4691	1:1000	Cytosolic	AB_915783
Rabbit polyclonal anti-IκBα	SCBT/ sc371	1:1000	Cytosolic	AB_2235952
Rabbit polyclonal anti-NF-κB p65	SCBT/ sc372	1:1000	Nuclear	AB_632037
Rabbit polyclonal anti-iNOS	SCBT/ sc650	1:750 (1% BSA)	Cytosolic	AB_2298577
Mouse monoclonal anti-4-hydroxynonenal	R&D Systems/ MAB3249	1:500 (3% BSA)	Cytosolic	AB_664165
Mouse monoclonal anti-Keap-1	R&D Systems/ MAB3024	1:1000	Cytosolic	AB_2132620
Rabbit polyclonal anti-Nrf2	SCBT/ sc722	1:1000	Nuclear	AB_2108502

Abbreviations: BSA, bovine serum albumin; CST, Cell Signaling Technology; SCBT, Santa Cruz Biotechnology.

2.6.3. TBARS

TBARS concentration in NAcc homogenates was quantiffed by the thiobarbituric acid method (Das and Ratty, 1987), which is described in SD.

2.6.4. MT quantification

MT I-II concentration was determined in NAcc homogenates. MT I-II was quantiffed with a modiffed Cd/hemoglobin saturation radioassay (Aburto-Luna et al., 2017; Arroyo-García et al., 2020) since these isoforms are the only ones sensitive to Cd (Braga et al., 2015; Palmiter et al., 1992). For details see SD.

2.6.5. Protein quantification

Protein levels were measured using the Bradford method based on the protein-dye binding principle (Bradford, 1976).

2.7. Statistical analyses

No software or method for sample size calculation was used, but the sample size for each probe is in accordance with literature reports. The mean values of each animal were treated as a single measurement for data analysis. All data in the ffgures are presented with the sample dispersion and as the mean ± SEM. Data analysis was assessed by trained personnel who were blinded to experimental conditions. After normal distribution veriffcation, data were analyzed using two-way ANOVA for total dendritic length, dendritic spine density, dendritic spine classiffcation, neuronal density, and biochemical assays, considering lesion and RISP treatment as independent factors. A three-way ANOVA was employed for data on length per dendritic order and dendritic arborization, considering lesion, RISP, and branch order or distance to soma as independent factors. If a signiffcant interaction was detected, the *post-hoc* Newman-Keuls test was assessed. In the graphs multiple comparison significance is indicated with asterisks or lowercase letters, the main lesion effect is indicated by α, RISP main effect is indicated by β, and interaction without significant multiple comparisons results is indicated by δ. The full statistical results are presented in Table 3. Regarding MT quantiffcation, data did not have a normal distribution and was analyzed using a Kruskal-Wallis probe followed by Dunn's test for multiple comparisons. In all cases, a p-value of 0.05 was considered the threshold for statistical significance. For data with $p > 0.05$ and considered significant, the p-value is indicated in the graph. Data analysis was carried out using GraphPad Prism 9.0.

3. Results

3.1. Verification of the lesion

Coronal sections at the level of the ventral hippocampus were obtained and stained with cresyl violet ($n = 88$, sham = 44, and NVHL = 44). Then, sections were analyzed, and only animals with limited ventral hippocampus bilateral lesions were included in the NVHL group. Sham animals did not show any macroscopic lesions or gliosis (Fig. 1B).

3.2. RISP treatment effects on the neuronal number in the NAcc in rats with NVHL

The NVHL did not alter the number of neurons in the NAcc, but ANOVA analysis revealed that RISP increased the number of neurons in both sham and NVHL animals in this region (Fig. 1D).

3.3. Effects of the RISP treatment in the SPNs structural plasticity of the NAcc in rats with NVHL

Morphological analysis of NAcc SPNs showed structural alterations in NVHL rats. The total dendritic length (Fig. 2C), the dendritic length in distal orders (Fig. 2D), and the dendritic arborization (Fig. 2E) decreased in the animals with NVHL. RISP administration recovered all the aforementioned parameters. Regarding the branch order length, the reduction was from the 2nd-4th in the NVHL-vehicle group, which RISP treatment restored (Fig. 2D). Concerning dendritic arborization, in the proximal levels (0-90 μm to soma) there were no differences in the vehicle or RISP-treated animals with NVHL, but in distal arbor (from 100 μm onwards to soma) RISP increased the arborization length (Fig. 2E). Moreover, the dendritic spine number and their morphology were analyzed. The NVHL reduced the number of dendritic spines, and RISP treatment restored it (Fig. 2G). Concerning the dendritic spine morphological classiffcation, the results are condensed in Fig. 2H. The NVHL reduced the population of mature dendritic spines (mushroom-like) in both vehicle and RISP-treated animals. However, RISP increased the number of mushroom spines as the main effect. The thin spine population remained unchanged. The number of stubby spines (with a less functional capability) increased in the NVHL rats in comparison with the sham animals in the vehicle-treated group, RISP does not affect this spine population. RISP decreased the number of bifurcated spines in the sham rats and increased it in the NVHL rats. Multiheaded spines increased in the sham-RISP group in comparison with all the other groups. Finally, the unclassiffed spine population remained unaffected by either NVHL or RISP treatment.

Table 3
Statistical results. Bold values indicate statistical significance.

Two-way ANOVA, independent factors: lesion and RISP, F values (DFn, DFd) and *p*-values

Parameter	Lesion	RISP treatment	Interaction
Stereology	F (1,12) = 1.243; $p = 0.2868$	**F (1, 12) = 4.424; $p = 0.0572$**	F (1, 12) = 1.205; $p = 0.2939$
Total dendritic length	**F (1, 28) = 23.42; $p < 0.0001$**	F (1, 28) = 0.928; $p = 0.3436$	**F (1, 28) = 8.207; $p = 0.0078$**
Number of spines	**F (1, 28) = 7.79; $p = 0.0094$**	**F (1, 28) = 12.74; $p = 0.0013$**	**F (1, 28) = 3.985; $p = 0.0557$**
Muhsroom spines	**F (1, 28) = 17.68; $p = 0.0002$**	**F (1, 28) = 5.633; $p = 0.0247$**	F (1, 28) = 1.581; $p = 0.219$
Thin spines	F (1, 28) = 0.02432; $p = 0.8772$	**F (1, 28) = 4.152; $p = 0.0511$**	**F (1, 28) = 3.902; $p = 0.0582$**
Stubby spines	**F (1, 28) = 3.345; $p = 0.0781$**	F (1, 28) = 0.04474; $p = 0.834$	**F (1, 28) = 9.293; $p = 0.005$**
Bifurcated spines	**F (1, 28) = 19.61; $p = 0.0001$**	F (1, 28) = 0.2199; $p = 0.6428$	**F (1, 28) = 20.54; $p < 0.0001$**
Multi-headed spines	**F (1, 28) = 15.77; $p = 0.0005$**	**F (1, 28) = 12.25; $p = 0.0016$**	**F (1, 28) = 23.48; $p < 0.0001$**
Unclassified spines	F (1, 28) = 0.1769; $p = 0.6773$	F (1, 28) = 1.365; $p = 0.2525$	F (1, 28) = 0.2643; $p = 0.6112$
Nitrites	**F (1, 16) = 7.107; $p = 0.0169$**	**F (1, 16) = 4.751; $p = 0.0446$**	**F (1, 16) = 5.424; $p = 0.0333$**
iNOS	F (1, 16) = 0.7969; $p = 0.3852$	**F (1, 16) = 47.57; $p < 0.0001$**	**F (1, 16) = 3.99; $p = 0.0631$**
TBARS	F (1, 16) = 0.7452; $p = 0.4007$	**F (1, 16) = 4.685; $p = 0.0459$**	F (1, 16) = 2.04; $p = 0.1724$
4HNE	F (1, 16) = 0.2961; $p = 0.5938$	F (1, 16) = 2.069; $p = 0.1696$	**F (1, 16) = 4.562; $p = 0.0485$**
IKBα	F (1, 16) = 2.921; $p = 0.1068$	**F (1, 16) = 8.444; $p = 0.0103$**	F (1, 16) = 0.3775; $p = 0.5476$
NF-κB (p65)	F (1, 16) = 1.979; $p = 0.1787$	F (1, 16) = 1.345; $p = 0.2631$	**F (1, 16) = 9.862; $p = 0.0063$**
pp38/p38α/β	**F (1, 16) = 6.306; $p = 0.0231$**	F (1, 16) = 2.208; $p = 0.1568$	**F (1, 16) = 6.395; $p = 0.0223$**
pJNK/JNK	F (1, 16) = 0.3941; $p = 0.5390$	F (1, 16) = 0.8835; $p = 0.3612$	F (1, 16) = 3.656; $p = 0.0739$
pERK/ERK	F (1, 16) = 0.207; $p = 0.6552$	**F (1, 16) = 4.544; $p = 0.0489$**	F (1, 16) = 1.013; $p = 0.3292$
pSmad-2/3/Smad-2/3	F (1, 16) = 2.95; $p = 0.1052$	F (1, 16) = 3.248; $p = 0.0904$	**F (1, 16) = 4.129; $p = 0.0591$**
Smad-4	F (1, 16) = 0.272; $p = 0.6091$	**F (1, 16) = 5.191; $p = 0.0368$**	F (1, 16) = 0.9405; $p = 0.3466$
PI3K	F (1, 16) = 0.0295; $p = 0.8658$	F (1, 16) = 0.2997; $p = 0.5916$	F (1, 16) = 0.02112; $p = 0.8863$
pAkt/Akt	F (1, 16) = 0.4786; $p = 0.499$	**F (1, 16) = 14.04; $p = 0.0018$**	F (1, 16) = 2.428; $p = 0.1388$
Keap-1	F (1, 16) = 1.018; $p = 0.3281$	F (1, 16) = 1.278; $p = 0.275$	F (1, 16) = 1.507; $p = 0.2373$
Nrf2	**F (1, 16) = 3.842; $p = 0.0676$**	**F (1, 16) = 8.144; $p = 0.0115$**	**F (1, 16) = 4.201; $p = 0.0572$**

Three-way ANOVA, independent factors: RISP, lesion, and branch order, F values (DFn, DFd) and *p*-values

Parameter	Lesion	RISP	Branch order
Length per branch order	**F (1, 14) = 19.47; $p = 0.0006$**	F (1, 14) = 2.423; $p = 0.1419$	**F (6, 84) = 708.1; $p < 0.0001$**
	Interactions		
	Lesion x RISP	Lesion x RISP x Branch order	
	F (1, 14) = 15.72; $p = 0.0014$	F (6, 84) = 1.48; $p = 0.195$	

Three-way ANOVA, independent factors: RISP, lesion, and distance to soma, F values (DFn, DFd) and *p*-values

Parameter	Lesion	RISP	Distance to soma
Arborization	**F (1, 14) = 17.79; $p = 0.0009$**	F (1, 14) = 1.357; $p = 0.2635$	**F (27, 378) = 2006; $p < 0.0001$**
	Interactions		
	Lesion x RISP	Lesion x RISP x Distance to soma	
	F (1, 14) = 12.00; $p = 0.0038$	**F (27, 378) = 2.015; $p = 0.0023$**	

3.4. Effects of the RISP treatment on O/NS in the striatum of rats with NVHL

Nitrite concentration increased as a consequence of the NVHL, and RISP reduced it to control levels (Fig. 3A). Protein levels of the inducible nitric oxide (NO) synthase (iNOS) decreased as a consequence of the RISP treatment in both sham and NVHL rats (Fig. 3B). O/NS was studied through the quantiffcation of lipid peroxidation-related molecules. TBARS concentration was reduced in both sham and NVHL animals treated with RISP (Fig. 3C). Regarding 4-hydroxy-2-nonenal (4-HNE) protein levels, ANOVA analysis revealed a signiffcant interaction between lesion and RISP without multiple comparison differences detected among groups (Fig. 3D).

3.5. Effects of the RISP treatment on the NF-κB pathway in the striatum of rats with NVHL

The nuclear factor-κB (NF-κB) pathway is a key component of the inflammatory response. NF-κB remains inactive in the cytosol by its union with the inhibitory subunit of the, IκBα (IκBα). Under pro-inflammatory conditions, NF-κB separates from IκBα, translocates to the nucleus, and stimulates the synthesis of pro-inflammatory mediators (Dresselhaus and Meffert, 2019). Cytosolic IκBα protein levels increased as a main effect of the RISP treatment (Fig. 3E). The nuclear NF-κB protein levels increased in the NVHL animals and were reduced to control levels after RISP treatment (Fig. 3F).

3.6. Effects of the RISP treatment on the MAPK pathways in the striatum of rats with NVHL

The mitogen-activated protein kinases (MAPK) are part of the Ser/Thr protein kinase family and are activated by diverse stimuli, including growth factor signaling and stress (Fukunaga and Miyamoto, 1998). The protein levels of the extracellular signal-regulated kinases 1 and 2 (ERK 1/2), Jun N-terminal kinase (JNK), and p38 kinase were evaluated. The protein levels of phosphorylated-p38/p38α/β ratio increased as a consequence of the NVHL, and RISP reduced it to control levels (Fig. 4A). Phosphorylated-JNK/JNK ratio protein levels remained unchanged (Fig. 4B). Finally, RISP increased the phosphorylated-ERK 1/2/ERK 1/2 ratio protein levels in sham and NVHL rats (Fig. 4C).

3.7. Effects of the RISP treatment on the Smad2/3 and Smad4 in the striatum of rats with NVHL

Smad2/3 and Smad4 proteins are part of the canonical transforming growth factor β (TGF-β) pathway, but also can be stimulated by MAPK (Moustakas and Heldin, 2005). After phosphorylation, Smad2/3 couples to Smad4, and this complex translocates to the nucleus to promote the synthesis of anti-inflammatory mediators. ANOVA analysis of phosphorylated-Smad-2/3/Smad-2/3 protein ratio revealed that interaction was near the statistical signiffcance threshold, but the multiple comparison test did not show any signiffcant result (Fig. 4D). RISP increased the Smad-4 protein levels in both

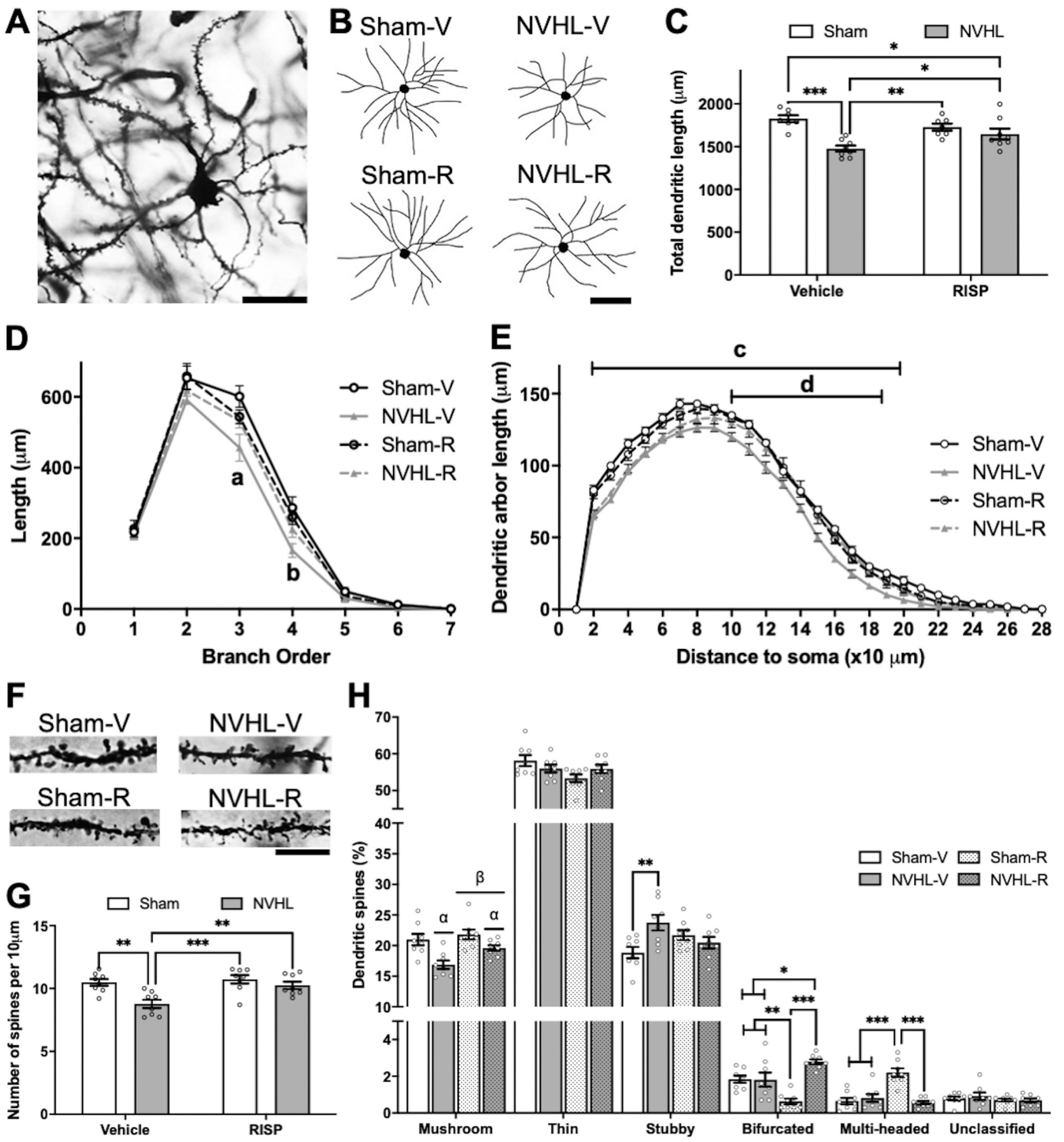

Fig. 2. Structural neuroplasticity of the SPNs of the NAcc ($n = 8$/group). A, representative photomicrograph of a SPN in the NAcc of the sham-vehicle group (scale bar = 50 μm). B, representative bidimensional neuronal reconstructions of SPNs in the NAcc of each experimental group (scale bar = 50 μm). C, NVHL reduced the total dendritic length of the SPNs, and RISP treatment recovered it (two-way ANOVA, *post-hoc* Newman-Keuls test: $^{*}p < 0.05$, $^{**}p < 0.01$, $^{***}p < 0.001$). D, NVHL reduced the 3rd and 4th branch order length of the SPNs, which RISP corrected (three-way ANOVA, *post-hoc* Newman-Keuls test: $^{a}p < 0.05$ Sham-Veh vs both RISP groups, $p < 0.01$ NVHL-Veh vs both RISP groups, $p < 0.0001$ NVHL-Veh vs Sham-Veh; $^{b}p < 0.01$ NVHL-Veh vs NVHL-RISP, $p < 0.01$ NVHL-Veh vs Sham-RISP, $p < 0.001$ NVHL-Veh vs Sham-Veh). E, NVHL reduced proximal and distal sections of the dendritic arbor, and RISP restored only the distal section length (three-way ANOVA, *post-hoc* Newman-Keuls test: $^{c}p < 0.05$ NVHL-Veh vs both Sham groups, $p < 0.05$ NVHL-RISP vs both Sham groups; $^{d}p < 0.05$ NVHL-Veh vs all the other groups). F, representative photomicrographs of dendritic sections of each group (scale bar = 10 μm). G, NVHL reduced the number of dendritic spines in the SPNs, which RISP restored (two-way ANOVA, *post-hoc* Newman-Keuls test: $^{**}p < 0.01$, $^{***}p < 0.001$). H, NVHL reduced the number of mushroom spines and RISP increased it, both as main effects (two-way ANOVA, $^{\alpha}$lesion main effect: 0.0002; $^{\beta}$RISP main effect: $p = 0.0247$). No changes were detected in the thin spine population. In the vehicle-treated rats, the NVHL increased the number of stubby spines increased in comparison with sham group (two-way ANOVA, *post-hoc* Newman-Keuls test: $^{**}p < 0.01$). Bifurcated spines decreased in the Sham RISP-treated rats and increased in the NVHL-RISP group (two-way ANOVA, *post-hoc* Newman-Keuls

test: *$p < 0.05$, **$p < 0.01$, ***$p < 0.001$). RISP treatment increased the number of multi-headed spines in the Sham rats (two-way ANOVA, *post-hoc* Newman-Keuls test: ***$p < 0.001$).

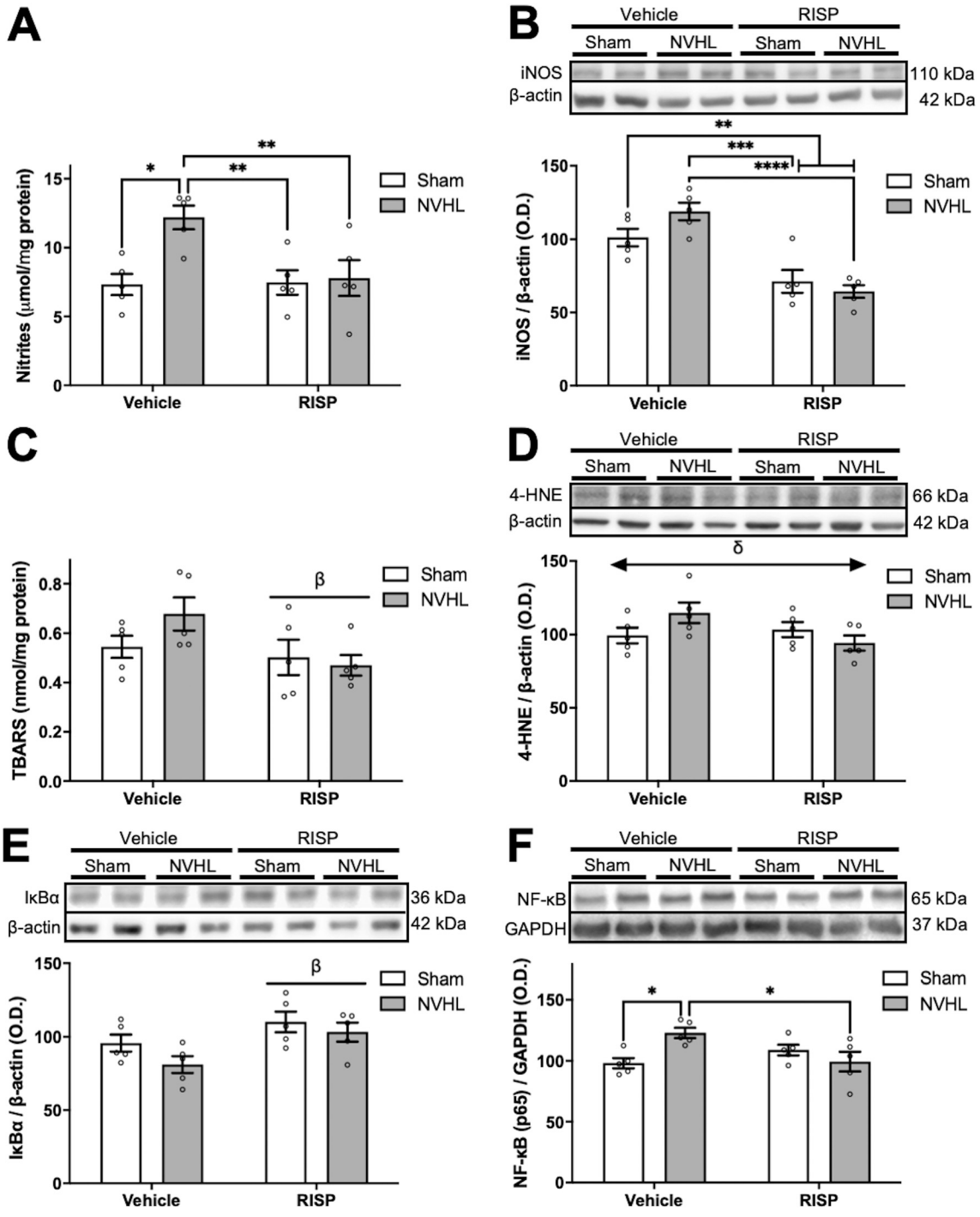

Fig. 3. NO pathway and oxidative/nitrosative stress (O/NS). Representative blots for each protein are shown ($n = 5$/group). A, B, NO pathway. A, the NVHL increased nitrite concentration in the vehicle-treated group and RISP-treatment reduced it to control levels (two-way ANOVA, *post-hoc* Newman-Keuls test: **$p < 0.01$, ***$p < 0.001$, ****$p < 0.0001$). B, RISP decreased the iNOS protein levels in both sham and NVHL animals (two-way ANOVA, *post-hoc* Newman-Keuls test: *$p < 0.05$, **$p < 0.01$). C, D, lipid peroxidation. C, RISP decreased the TBARS concentration as the main effect (two-way ANOVA, $^{\beta}$RISP main effect: $p = 0.0459$). D, regarding 4-HNE protein levels, although significant interaction was detected no differences were detected among groups (two-way ANOVA, $^{\delta}$lesion × RISP interaction: $p = 0.0485$). F, G, NF-κB pathway. F, RISP increased IκBα protein levels in both sham and NVHL animals (two-way ANOVA, $^{\beta}$RISP main effect: $p = 0.0103$). G, NVHL increased NF-κB protein levels and RISP treatment reduced it to control levels (two-way ANOVA, *post-hoc* Newman-Keuls test: *$p < 0.05$).

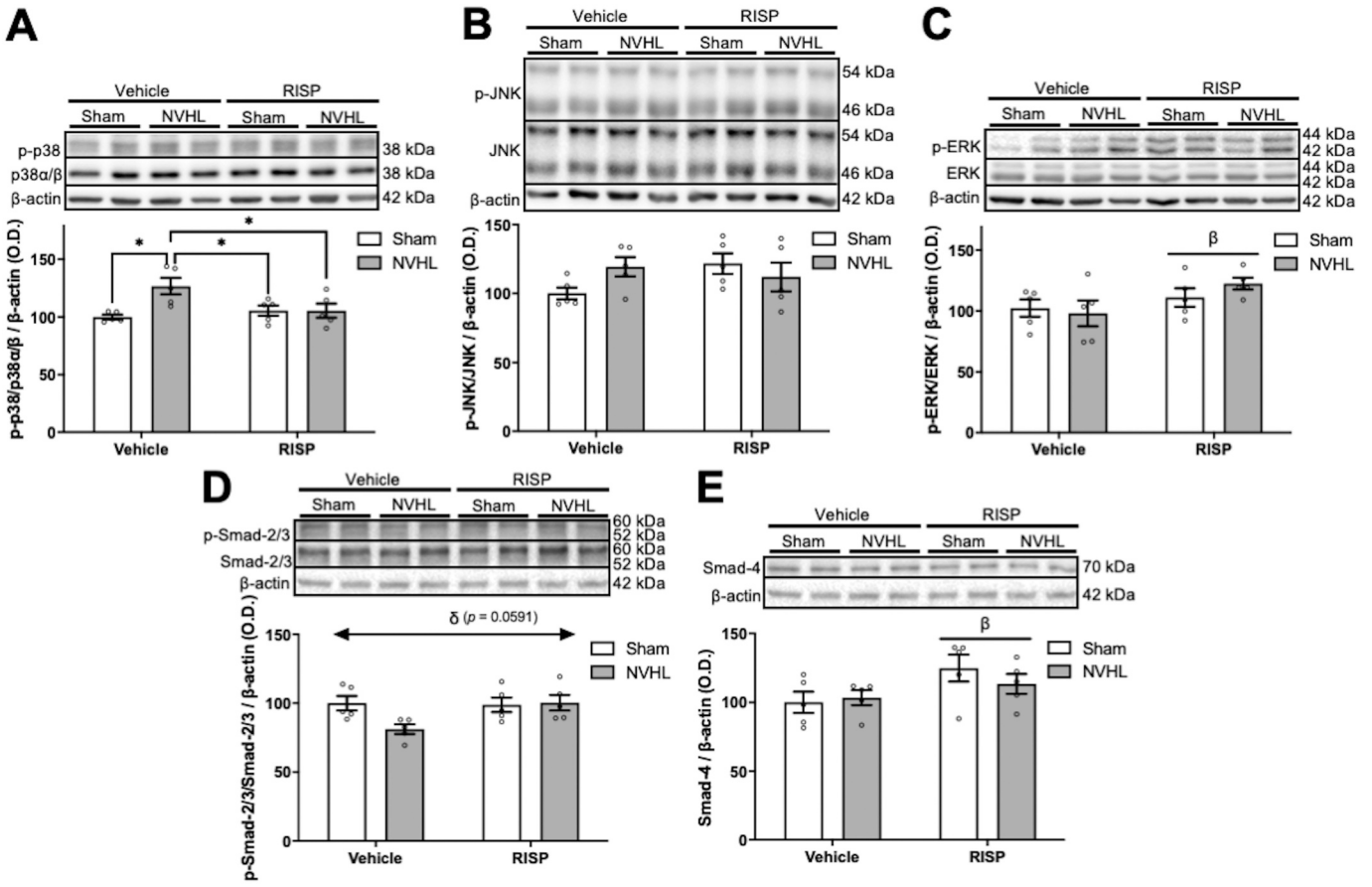

Fig. 4. MAPK and Smad pathways. Representative blots for each protein are shown (n = 5/group). A–C, MAPK pathway. A, NVHL increased p38 ratio and RISP treatment reduced it to control levels (two-way ANOVA, *post-hoc* Newman-Keuls test: $^{*}p < 0.05$). B, JNK ratio did not change. C, RISP increased the ERK ratio in both sham and NVHL animals (two-way ANOVA, $^{\beta}$RISP main effect: $p = 0.0489$). D, E, Smad pathway. D, regarding the Smad-2/3 ratio, the interaction *p*-value was near the statistical significance threshold (two-way ANOVA, $^{\delta}$lesion × RISP interaction, $p = 0.0591$). E, RISP increased Smad-4 protein levels in both sham and NVHL animals (two-way ANOVA, $^{\beta}$RISP main effect: $p = 0.0368$).

sham and NVHL animals (Fig. 4E).

3.8. Effects of the RISP treatment on the PI3K/Akt pathway in the striatum of rats with NVHL

Phosphoinositide 3-kinase/protein kinase B (PI3K/Akt) signaling is involved in neuroplasticity, cell surveillance, and antioxidant response (Kitagishi et al., 2012). PI3K protein levels did not change among experimental groups (Fig. 5A). Interestingly, phosphorylated-Akt/Akt ratio protein levels increased in both sham and NVHL animals treated with RISP (Fig. 5B).

3.9. Effects of the RISP treatment on the Nrf2 pathway in the striatum of rats with NVHL

The nuclear factor (erythroid-derived 2)-like 2 (Nrf2) pathway is one of the main antioxidant enzyme sources in the CNS. Nrf2 nuclear translocation is regulated by the PI3K, which promotes the separation of the Kelch-like ECH-associated protein 1 (Keap-1), the cytosolic inhibitor of Nrf2 (Ma, 2013). Cytosolic Keap-1 remained unchanged among groups (Fig. 5C). However, nuclear Nrf2 protein levels were reduced as a consequence of the NVHL and increased to control levels after RISP treatment (Fig. 5D). Nrf2 nuclear translocation promotes the synthesis of antioxidant enzymes including MT I-II (Paladino et al., 2018). MT I-II increased in the NVHL RISP-treated rats in comparison with the NVHL animals treated with vehicle (Kruskal-Wallis test = 10.09, $p = 0.0179$, Dunn's test for multiple comparisons: $p = 0.0117$, Fig. 5E).

4. Discussion

Our results indicate that NVHL atrophies the structural neuroplasticity of the SPNs in the NAcc, without affecting the number of neurons in this area. Also, the NVHL increases the pro-infiammatory p38 MAPKs and NF-κB pathways, which may lead to O/NS evidenced by the lipid peroxidation. Impairments in the Nrf2 antioxidant pathway can be also related to O/NS. RISP treatment (0.25 mg/kg, i.p.) for 21 consecutive days enhances the dendritic arbor length and the number of dendritic spines (through the increase in the mature spines) in the SPNs in NVHL young-adult male rats. Moreover, RISP decreases the pro-inflammatory p38 MAPK and NF-κB pathways and seems to increase the anti-inflammatory Smad-2/3/Smad-4 signaling. NO concentration and iNOS protein levels, as well as lipid peroxidation, were also reduced as a consequence of RISP treatment. Finally, RISP restored the Nrf2 antioxidant pathway and increased the concentration of the MT I-II antioxidant enzymes in the NVHL animals.

The mesolimbic dopaminergic dysfunction in the NVHL model impairs the PFC (O'Donnell, 2002). PFC dysfunction disrupts the PFC-ventral hippocampus-NAcc circuit, triggering behavioral alterations related to SZ-symptoms such as reduced social interplay, working memory deffcits, or hypersensitivity to psychostimulants/stress (Brady, 2009; Brady et al., 2010). Thus, SPN atrophy may be a consequence of altered dopaminergic (from VTA) and glutamatergic (PFC-ventral hippocampus) inputs in the NAcc. RISP treatment restored it, allowing structural plasticity in SPNs, maybe through the depolarization block phenomena in the VTA axons, which modulates the dopaminergic mesolimbic activity (Grace, 1997); or through the modulation of synaptic and cytoskeleton protein expression (Kedracka-Krok et al., 2016).

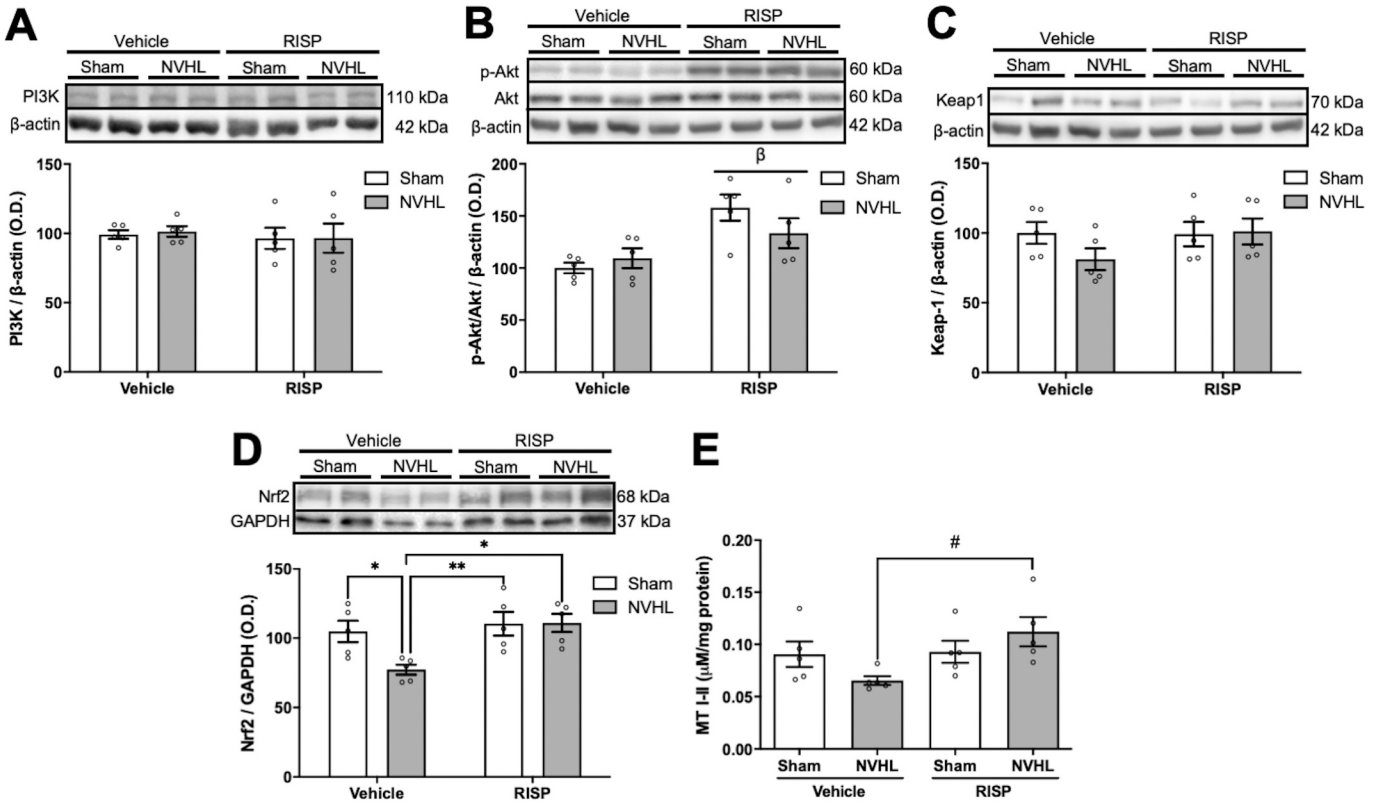

Fig. 5. PI3K/Akt and Nrf2 pathways, and MT I-II concentration (n = 5/group). Representative blots for each protein are shown (A–D). A, B, PI3K/Akt pathway. A, no changes in the PI3K protein levels were detected among groups. B, RISP increased the protein Akt ratio as the main effect (two-way ANOVA, $^{\beta}$RISP main effect: $p = 0.0018$). C-E, Nrf2 pathway. C, no changes in the Keap-1 protein levels were detected among groups. D, in the NVHL animals, Nrf2 protein levels decreased and RISP treatment increased them to control level (two-way ANOVA, *post-hoc* Newman-Keuls test: $^{*}p < 0.05$, $^{**}p < 0.01$). E, MT I-II concentration was quantified by Cd radioimmunoassay. In rats with NVHL, MT I-II concentration was higher in the RISP-treated animals compared to the vehicle-treated ones (Kruskal-Wallis test, *post-hoc* Dunn's test: $^{\#}p = 0.0117$).

However, our results suggest that infiammatory and antioxidant/oxidant substance imbalance may also be contributing to the structural neuroplasticity alterations of the SPNs of the NAcc in NVHL rats.

It has been demonstrated that chronic administration of dopaminergic agonists such as amphetamine, apomorphine, or cocaine not only induce an SZ-like behavioral phenotype in rodents, but also reduces the number of neurons, alters neuroplasticity, and induces O/NS in limbic brain areas (Arroyo-García et al., 2020, 2018; Hawken and Beninger, 2014; Robinson and Kolb, 1999; Tendilla-Beltrán et al., 2016). NVHL rats have functional dopaminergic hyperactivity in the striatum (Bhardwaj et al., 2003; Vázquez-Roque et al., 2012), which may be leading to infiammation, O/NS, and consequently to cell death. Interestingly, the NVHL did not reduce the number of neurons in the NAcc as it does in the PFC (Tendilla-Beltrán et al., 2019b; Vázquez-Roque et al., 2012) and the amygdala (Vázquez-Roque et al., 2014). There is a trend of RISP to increase the number of neurons in the NAcc in both sham and NVHL rats. These results can be explained by striatal adult neurogenesis, which is modulated by dopaminergic receptors of the D2 family (Diaz et al., 1997; Winner et al., 2009); or because of the reduced density of striatal fast-spiking parvalbumin-positive interneurons compared to the neocortex (Fitzgerald et al., 2011), and these cells seem to be vulnerable to O/NS because of their high metabolic rate (Steullet et al., 2017). However, further studies must analyze whether AADs promote striatal neurogenesis, as they do in the hippocampus (Chikama et al., 2017). Thus, speciffcally in the striatum of the NVHL animals, the infiammatory imbalance and its consequences may be implicated in the rearrangement of the synaptic surface of the SPNs.

One molecule that has both neuroplasticity and infiammatory effects is NO. NO is essential for synaptic transmission by modulating the presynaptic neurotransmitter liberation. The production of NO for this purpose is through the constitutive neuronal NO synthase (nNOS) and endothelial NO synthase (eNOS) (Blackshaw et al., 2003). NO concentration increases under infiammatory response through iNOS activity (Brown, 2007), since iNOS synthesis is induced by NF-κB and its activity is stimulated by pro-infiammatory cytokines (Aktan, 2004). RISP treatment corrected the increased NF-κB nuclear protein levels, suggesting the downregulation of this pathway and consequently the reduction of pro-infiammatory molecules such as NO. Because of its high reactivity, NO can lead to forming other free radicals and reactive molecules such as peroxynitrite and consequently membrane damage through phospholipid peroxidation (Hogg and Kalyanaraman, 1999). Lipid peroxidation is a consequence of O/NS, which stimulates several signaling pathways related to infiammatory response, such as the MAPK. Bychkov et al. (2011) demonstrated decreased ERK and Akt protein levels in the NAcc of adult male NVHL rats, suggesting a role in congruence with the upregulation exerted by RISP in our present results. Among the MAPK, p38 and JNK have been associated with a pro-infiammatory state, as happened in the striatum of NVHL rats with p38, which RISP treatment reduced.

Also, JNK and ERK MAPK can stimulate the Smad pathway, which is associated with anti-infiammatory cytokine synthesis. JNK expression did not change in our experiment, but RISP induced ERK. The protein levels of the Smad-2/3 ratio decreased in the NVHL animals, which RISP treatment augmented in these rats. Moreover, RISP increased the Smad-4 protein levels, suggesting that RISP may be promoting the synthesis of anti-infiammatory mediators. Joseph et al. (2018), reported that TGF-β1 administration from P7 to P14 enhanced structural neuroplasticity and reduced the expression of the pro-infiammatory cytokine interleukin 1 β in the PFC, as well as corrected the behavioral abnormalities of adult NVHL rats. Thus, RISP may stimulate the TGF-β pathway in the striatum and consequently help to ameliorate the neuronal atrophy and the infiammation in the rats with NVHL. However,

further studies must study this pathway to clarify in which manner AADs act on the TGF-β pathway.

O/NS also stimulates compensatory mechanisms such as the antioxidant response via Nrf2 activity. Nrf2 prompts the synthesis of various antioxidant molecules for detoxiffcation, cellular redox balance, and heme/metal metabolism (Paladino et al., 2018). In this last category, in the brain, MT I-II are poorly studied antioxidant proteins, since MT III is the most abundant isoform (also known as growth inhibitory factor) (Palmiter et al., 1992). MT I-II's main function is to chelate essential and non-essential metals, and their binding with transition metals such as Fe and Cu exerts an antioxidant effect. But also it has been suggested that MT I-II can sequester free radicals (Ruttkay-Nedecky et al., 2013). Also, paliperidone, which is the

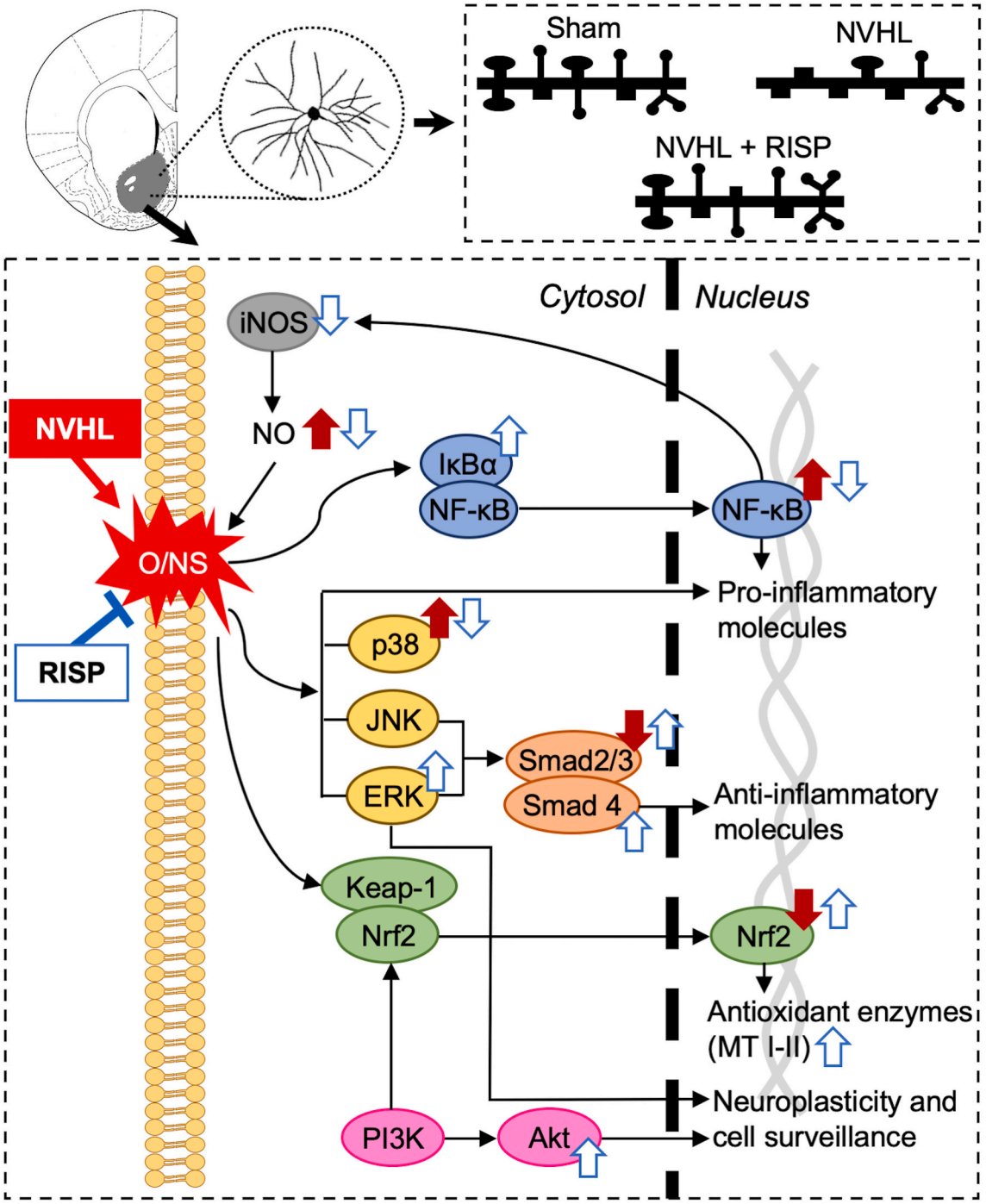

Fig. 6. Schematic representation of the results. In the NAcc of NVHL rats, SPNs are atrophied and have a dendritic spine pathology. RISP treatment ameliorates structural plasticity SPN impairments by restoring the number of dendritic spines as well as the number of mushroom spines. Also, NVHL (solid red arrows) generates oxidative/nitrosative stress (O/NS), which may be a consequence of the excessive NO concentration promoted by the NF-κB. O/NS stimulates the expression of pro-inflammatory MAPK: p38 and JNK. Decreased protein levels of the Smad signaling proteins may be disrupting the anti-inflammatory response. Moreover, the reduced levels of the Nrf2 may compromise the antioxidant response. RISP (blue outline arrows) diminished the O/NS and the NO concentration, as well as iNOS and NF-κB protein levels in the NVHL animals. Also, RISP reduced the levels of pro-inflammatory mediator p38; but increased ERK and Akt protein levels, which may exert enhancement neuroplasticity effects. Additionally, RISP restored Nrf2 protein levels and increased MT I-II concentration, which is an antioxidant molecule. (For interpretation of the references to colour in this figure legend, the reader is referred to the web version of this article.)

active metabolite of RISP, increased the Nrf2-related antioxidant enzymes in the PFC of rats subjected to acute stress (MacDowell et al., 2016). Here, we found that RISP increases the nuclear Nrf2 protein levels (probably through the RISP effects on its activator p-Akt) and the MT I-II concentration in the NVHL rats. Thus, RISP may be attenuating O/NS in the striatum by the reduction of NO concentration, NF-κB activity, and p38 MAPK, as well as by the restoration of the Nrf2 and Smad2/3 pathways. Fig. 6 schematically represents all the present results.

Bychkov et al. (2011) reported sex differences in the expression of MAPK in the striatum of NVHL rats. Here arises a limitation of this study, since it was only used male rats. Although most of the behavioral, neurochemical, and neuroplasticity data of the NVHL has been obtained from males; including females in this study could have been interesting to explore the sex differences of AAD treatment on these parameters and neuroplasticity.

5. Conclusion

In rats with NVHL, which is a SZ-related developmental model, RISP administration improves the structural neuroplasticity of SPNs in the NAcc, enhances the Nrf2 pathway, and modulates the NO, the NF-κB, and the MAPK pathways. These effects may be contributing to the previously found cognitive performance improvement of the animals with NVHL (Tendilla-Beltrán et al., 2019b). This reinforces the hypothesis that AADs enhance the brain function and improve behavioral performance in SZ beyond their monoaminergic mechanisms.

Fundings

This work was supported by the Spanish Ministry of Economy, Industry and Competitiveness (MINECO-EU-FEDER) SAF2016-75500-R to JCL and PRODEP (CA-BUAP-120) and the CONACYT Grant (252808) to GF. None of the funding institutions had any further role in the study design, the collection of data, analyses, and interpretation of data, writing of the report, or in the decision to submit the paper for publication.

CRediT authorship contribution statement

HT-B, JCL, and GF designed the study and wrote the protocol. H-TB, HC-C, SM-P, EB, and DM-H performed the experiments. HT-B, RAV-R, MT-R, LG-R, JLMM, JCL, and GF analyzed data. HT-B, JCL, and GF wrote the paper.

Aknowledgements

HT-B and HC-C acknowledge CONACYT for doctoral scholarship; and RAV-R, EB, MT-R, LG-R, and GF acknowledge the "Sistema Nacional de Investigadores" of Mexico for memberships. We thank Francisco Ramos Collazo for animal care, Sandra Rodriguez-Maus for biochemical experiment assistance, Jorge Armando Guzmán Vélez for neuronal morphology analyses, and Robert Simpson for English language revision.

Declaration of competing interest

None.

Appendix A. Supplementary data

Supplementary data to this article can be found online at https://doi.org/10.1016/j.schres.2021.07.014.

References

Abi-Dargham, A., Rodenhiser, J., Printz, D., Zea-Ponce, Y., Gil, R., Kegeles, L.S., Weiss, R., Cooper, T.B., Mann, J.J., Van Heertum, R.L., Gorman, J.M., Laruelle, M., 2000. Increased baseline occupancy of D2 receptors by dopamine in schizophrenia. Proc. Natl. Acad. Sci. U. S. A. 97, 8104–8109. https://doi.org/10.1073/pnas.97.14.8104.

Aburto-Luna, V., Treviño, S., Santos-López, G., Moroni-González, D., Calva-Cruz, O., Aguilar-Alonso, P., León-Chávez, B.A., Brambila, E., 2017. Hepatic mobilization of zinc after an experimental surgery, and its relationship with inflammatory cytokines release, and expression of metallothionein and Zip14 transporter. Inflamm. Res. 66, 167–175. https://doi.org/10.1007/s00011-016-1003-5.

Aktan, F., 2004. iNOS-mediated nitric oxide production and its regulation. Life Sci. 75, 639–653. https://doi.org/10.1016/j.lfs.2003.10.042.

Alberquilla, S., Gonzalez-Granillo, A., Martín, E.D., Moratalla, R., 2020. Dopamine regulates spine density in striatal projection neurons in a concentration-dependent manner. Neurobiol. Dis. 134, 104666 https://doi.org/10.1016/j.nbd.2019.104666.

Arroyo-García, L.E., Tendilla-Beltrán, H., Vázquez-Roque, R.A., Jurado-Tapia, E.E., Díaz, A., Aguilar-Alonso, P., Brambila, E., Monjaraz, E., De La Cruz, F., Rodríguez-Moreno, A., Flores, G., 2020. Amphetamine sensitization alters hippocampal neuronal morphology and memory and learning behaviors. Mol. Psychiatry. https://doi.org/10.1038/s41380-020-0809-2.

Arroyo-García, L.E., Vázquez-Roque, R.A., Díaz, A., Treviño, S., De La Cruz, F., Flores, G., Rodríguez-Moreno, A., 2018. The effects of non-selective dopamine receptor activation by apomorphine in the mouse hippocampus. Mol. Neurobiol. 55, 8625–8636. https://doi.org/10.1007/s12035-018-0991-2.

Bhardwaj, S.K., Beaudry, G., Quirion, R., Levesque, D., Srivastava, L.K., 2003. Neonatal ventral hippocampus lesion leads to reductions in nerve growth factor inducible-B mRNA in the prefrontal cortex and increased amphetamine response in the nucleus accumbens and dorsal striatum. Neuroscience 122, 669–676. https://doi.org/10.1016/j.neuroscience.2003.08.016.

Blackshaw, S., Eliasson, M.J.L., Sawa, A., Watkins, C.C., Krug, D., Gupta, A., Arai, T., Ferrante, R.J., Snyder, S.H., 2003. Species, strain and developmental variations in hippocampal neuronal and endothelial nitric oxide synthase clarify discrepancies in nitric oxide-dependent synaptic plasticity. Neuroscience 119, 979–990. https://doi.org/10.1016/S0306-4522(03)00217-3.

Bradford, M.M., 1976. A rapid and sensitive method for the quantitation of microgram quantities of protein utilizing the principle of protein-dye binding. Anal. Biochem. 72, 248–254. https://doi.org/10.1016/0003-2697(76)90527-3.

Brady, A.M., 2009. Neonatal ventral hippocampal lesions disrupt set-shifting ability in adult rats. Behav. Brain Res. 205, 294–298. https://doi.org/10.1016/j.bbr.2009.07.025.

Brady, A.M., Saul, R.D., Wiest, M.K., 2010. Selective deficits in spatial working memory in the neonatal ventral hippocampal lesion rat model of schizophrenia. Neuropharmacology 59, 605–611. https://doi.org/10.1016/j.neuropharm.2010.08.012.

Braga, M.M., Dick, T., de Oliveira, D.L., Scopel-Guerra, A., Mussulini, B.H.M., Souza, D. O., da Rocha, J.B.T., 2015. Evaluation of zinc effect on cadmium action in lipid peroxidation and metallothionein levels in the brain. Toxicol. Rep. 2, 858–863. https://doi.org/10.1016/j.toxrep.2015.05.014.

Bringas, M.E., Morales-Medina, J.C., Flores-Vivaldo, Y., Negrete-Diaz, J.V., Aguilar-Alonso, P., León-Chávez, B.A., Lazcano-Ortiz, Z., Monroy, E., Rodríguez-Moreno, A., Quirion, R., Flores, G., 2012. Clozapine administration reverses behavioral, neuronal, and nitric oxide disturbances in the neonatal ventral hippocampus rat. Neuropharmacology 62, 1848–1857. https://doi.org/10.1016/j.neuropharm.2011.12.008.

Brown, G.C., 2007. Mechanisms of inflammatory neurodegeneration: INOS and NADPH oxidase. Biochem. Soc. Trans. 35, 1119–1121. https://doi.org/10.1042/BST0351119.

Bychkov, E., Ahmed, M.R., Gurevich, E.V., 2011. Sex differences in the activity of signalling pathways and expression of G-protein-coupled receptor kinases in the neonatal ventral hippocampal lesion model of schizophrenia. Int. J. Neuropsychopharmacol. 14, 1–15. https://doi.org/10.1017/S1461145710000118.

Chikama, K., Yamada, H., Tsukamoto, T., Kajitani, K., Nakabeppu, Y., Uchimura, N., 2017. Chronic atypical antipsychotics, but not haloperidol, increase neurogenesis in the hippocampus of adult mouse. Brain Res. 1676, 77–82. https://doi.org/10.1016/j.brainres.2017.09.006.

Das, N.P., Ratty, A.K., 1987. Studies on the effects of the narcotic alkaloids, cocaine, morphine, and codeine on nonenzymatic lipid peroxidation in rat brain mitochondria. Biochem. Med. Metab. Biol. 37, 258–264. https://doi.org/10.1016/0885-4505(87)90035-1.

Diaz, J., Ridray, S., Mignon, V., Griffon, N., Schwartz, J.C., Sokoloff, P., 1997. Selective expression of dopamine D3 receptor mRNA in proliferative zones during embryonic development of the rat brain. J. Neurosci. 17, 4282–4292. https://doi.org/10.1523/jneurosci.17-11-04282.1997.

Dresselhaus, E.C., Meffert, M.K., 2019. Cellular specificity of NF-?B function in the nervous system. Front. Immunol. 10 https://doi.org/10.3389/fimmu.2019.01043.

Fitzgerald, M.L., Lupica, C.R., Pickel, V.M., 2011. Decreased parvalbumin immunoreactivity in the cortex and striatum of mice lacking the CB1 receptor. Synapse 65, 827–831. https://doi.org/10.1002/syn.20911.

Flores, G., Alquicer, G., Silva-Gómez, A.B., Zaldivar, G., Stewart, J., Quirion, R., Srivastava, L.K., 2005. Alterations in dendritic morphology of prefrontal cortical and nucleus accumbens neurons in post-pubertal rats after neonatal excitotoxic lesions of the ventral hippocampus. Neuroscience 133, 463–470. https://doi.org/10.1016/j.neuroscience.2005.02.021.

Flores, G., Barbeau, D., Quirion, R., Srivastava, L.K., 1996. Decreased binding of dopamine D3 receptors in limbic subregions after neonatal bilateral lesion of rat hippocampus. J. Neurosci. 16, 2020–2026. https://doi.org/10.1523/JNEUROSCI.16-06-02020.1996.

Fukunaga, K., Miyamoto, E., 1998. Role of MAP kinase in neurons. Mol. Neurobiol. 16, 79–95. https://doi.org/10.1007/BF02740604.

Gibb, R., Kolb, B., 1998. A method for vibratome sectioning of golgi-cox stained whole rat brain. J. Neurosci. Methods 79, 1–4. https://doi.org/10.1016/S0165-0270(97)00163-5.
Grace, A., 1997. Dopamine-cell depolarization block as a model for the therapeutic actions of antipsychotic drugs. Trends Neurosci. 20, 31–37. https://doi.org/10.1016/S0166-2236(96)10064-3.
Green, L.C., Wagner, D.A., Glogowski, J., Skipper, P.L., Wishnok, J.S., Tannenbaum, S.R., 1982. Analysis of nitrate, nitrite, and [15N]nitrate in biological fluids. Anal. Biochem. 126, 131–138. https://doi.org/10.1016/0003-2697(82)90118-X.
Hawken, E.R., Beninger, R.J., 2014. The amphetamine sensitization model of schizophrenia symptoms and its effect on schedule-induced polydipsia in the rat. Psychopharmacology 231, 2001–2008. https://doi.org/10.1007/s00213-013-3345-9.
Hendouei, N., Farnia, S., Mohseni, F., Salehi, A., Bagheri, M., Shadfar, F., Barzegar, F., Hoseini, S.D., Charati, J.Y., Shaki, F., 2018. Alterations in oxidative stress markers and its correlation with clinical findings in schizophrenic patients consuming perphenazine, clozapine and risperidone. Biomed. Pharmacother. 103, 965–972. https://doi.org/10.1016/j.biopha.2018.04.109.
Hogg, N., Kalyanaraman, B., 1999. Nitric oxide and lipid peroxidation. Biochim. Biophys. Acta Bioenerg. 1411, 378–384. https://doi.org/10.1016/S0005-2728(99)00027-4.
Joseph, A.T., Bhardwaj, S.K., Srivastava, L.K., 2018. Role of prefrontal cortex anti- and pro-inflammatory cytokines in the development of abnormal behaviors induced by disconnection of the ventral hippocampus in neonate rats. Front. Behav. Neurosci. 12, 244. https://doi.org/10.3389/fnbeh.2018.00244.
Kedracka-Krok, S., Swiderska, B., Jankowska, U., Skupien-Rabian, B., Solich, J., Dziedzicka-Wasylewska, M., 2016. Stathmin reduction and cytoskeleton rearrangement in rat nucleus accumbens in response to clozapine and risperidone treatment - comparative proteomic study. Neuroscience 316, 63–81. https://doi.org/10.1016/j.neuroscience.2015.12.028.
Kitagishi, Y., Kobayashi, M., Kikuta, K., Matsuda, S., 2012. Roles of PI3K/AKT/GSK3/mTOR pathway in cell signaling of mental illnesses. Depress. Res. Treat. 2012 https://doi.org/10.1155/2012/752563.
Lipska, B.K., Jaskiw, G.E., Weinberger, D.R., 1993. Postpubertal emergence of hyperresponsiveness to stress and to amphetamine after neonatal excitotoxic hippocampal damage: a potential animal model of schizophrenia. Neuropsychopharmacology 9, 67–75. https://doi.org/10.1038/npp.1993.44.
Ma, Q., 2013. Role of Nrf2 in oxidative stress and toxicity. Annu. Rev. Pharmacol. Toxicol. 53, 401–426. https://doi.org/10.1146/annurev-pharmtox-011112-140320.
MacDowell, K.S., Caso, J.R., Martín-Hernández, D., Moreno, B.M., Madrigal, J.L.M., Micó, J.A., Leza, J.C., García-Bueno, B., 2016. The atypical antipsychotic paliperidone regulates endogenous Antioxidant/Anti-inflammatory pathways in rat models of acute and chronic restraint stress. Neurotherapeutics 13, 833–843. https://doi.org/10.1007/s13311-016-0438-2.
MacDowell, K.S., García-Bueno, B., Madrigal, J.L.M., Parellada, M., Arango, C., Micó, J. A., Leza, J.C., 2013. Risperidone normalizes increased inflammatory parameters and restores anti-inflammatory pathways in a model of neuroinflammation. Int. J. Neuropsychopharmacol. 16, 121–135. https://doi.org/10.1017/S1461145711001775.
Martín-Hernández, D., Pereira, M.P., Tendilla-Beltrán, H., Madrigal, J.L.M., García-Bueno, B., Leza, J.C., Caso, J.R., 2019a. Modulation of monoaminergic systems by antidepressants in the frontal cortex of rats after chronic mild stress exposure. Mol. Neurobiol. 56, 7522–7533. https://doi.org/10.1007/s12035-019-1619-x.
Martín-Hernández, D., Tendilla-Beltrán, H., Madrigal, J.L.M., García-Bueno, B., Leza, J. C., Caso, J.R., 2019b. Chronic mild stress alters kynurenine pathways changing the glutamate neurotransmission in frontal cortex of rats. Mol. Neurobiol. 56, 490–501. https://doi.org/10.1007/s12035-018-1096-7.
Martinez-Cengotitabengoa, M., MacDowell, K.S., Alberich, S., Diaz, F.J., Garcia-Bueno, B., Rodriguez-Jimenez, R., Bioque, M., Berrocoso, E., Parellada, M., Lobo, A., Saiz, P.A., Matute, C., Bernardo, M., Gonzalez-Pinto, A., Leza, J.C., 2015. BDNF and NGF signalling in early phases of psychosis: relationship with inflammation and response to antipsychotics after 1 year. Schizophr. Bull. 42, 142–151. https://doi.org/10.1093/schbul/sbv078.
McCutcheon, R.A., Abi-Dargham, A., Howes, O.D., 2019. Schizophrenia, dopamine and the striatum: from biology to symptoms. Trends Neurosci. 42, 205–220. https://doi.org/10.1016/j.tins.2018.12.004.
Meltzer, H.Y., Massey, B.W., 2011. The role of serotonin receptors in the action of atypical antipsychotic drugs. Curr. Opin. Pharmacol. 11, 59–67. https://doi.org/10.1016/j.coph.2011.02.007.
Monfil, T., Vázquez Roque, R.A., Camacho-Abrego, I., Tendilla-Beltran, H., Iannitti, T., Meneses-Morales, I., Aguilar-Alonso, P., Flores, G., Morales-Medina, J.C., 2018. Hyper-response to novelty increases c-fos expression in the hippocampus and prefrontal cortex in a rat model of schizophrenia. Neurochem. Res. 43, 441–448. https://doi.org/10.1007/s11064-017-2439-x.
Monroy, E., Diaz, A., Tendilla-Beltrán, H., de la Cruz, F., Flores, G., 2020. Bexarotene treatment increases dendritic length in the nucleus accumbens without change in the locomotor activity and memory behaviors, in old mice. J. Chem. Neuroanat. 104, 101734 https://doi.org/10.1016/j.jchemneu.2019.101734.
Moustakas, A., Heldin, C.H., 2005. Non-smad TGF-ß signals. J. Cell Sci. 118, 3573–3584. https://doi.org/10.1242/jcs.02554.
O'Donnell, P., 2002. Neonatal hippocampal damage alters electrophysiological properties of prefrontal cortical neurons in adult rats. Cereb. Cortex 12, 975–982. https://doi.org/10.1093/cercor/12.9.975.
O'Donnell, P., Grace, A.A., 1995. Synaptic interactions among excitatory afferents to nucleus accumbens neurons: hippocampal gating of prefrontal cortical input. J. Neurosci. 15, 3622–3639. https://doi.org/10.1523/jneurosci.15-05-03622.1995.
Paladino, S., Conte, A., Caggiano, R., Pierantoni, G.M., Faraonio, R., 2018. Nrf2 pathway in age-related neurological disorders: insights into MicroRNAs. Cell. Physiol. Biochem. 47, 1951–1976. https://doi.org/10.1159/000491465.
Palmiter, R.D., Findley, S.D., Whitmore, T.E., Durnam, D.M., 1992. MT-III, a brain-specific member of the metallothionein gene family. Proc. Natl. Acad. Sci. 89, 6333–6337. https://doi.org/10.1073/pnas.89.14.6333.
Roberts, D.J., Strange, P.G., 2005. Mechanisms of inverse agonist action at D 2 dopamine receptors. Br. J. Pharmacol. 145, 34–42. https://doi.org/10.1038/sj.bjp.0706073.
Robinson, T.E., Kolb, B., 1999. Alterations in the morphology of dendrites and dendritic spines in the nucleus accumbens and prefrontal cortex following repeated treatment with amphetamine or cocaine. Eur. J. Neurosci. 11, 1598–1604. https://doi.org/10.1046/j.1460-9568.1999.00576.x.
Robinson, T.E., Kolb, B., 1997. Persistent structural modifications in nucleus accumbens and prefrontal cortex neurons produced by previous experience with amphetamine. J. Neurosci. 17, 8491–8497. https://doi.org/10.1523/JNEUROSCI.17-21-08491.1997.
Rueter, L.E., Ballard, M.E., Gallagher, K.B., Basso, A.M., Curzon, P., Kohlhaas, K.L., 2004. Chronic low dose risperidone and clozapine alleviate positive but not negative symptoms in the rat neonatal ventral hippocampal lesion model of schizophrenia. Psychopharmacology 176, 312–319. https://doi.org/10.1007/s00213-004-1897-4.
Ruttkay-Nedecky, B., Nejdl, L., Gumulec, J., Zitka, O., Masarik, M., Eckschlager, T., Stiborova, M., Adam, V., Kizek, R., 2013. The role of metallothionein in oxidative stress. Int. J. Mol. Sci. 14, 6044–6066. https://doi.org/10.3390/ijms14036044.
Sholl, D.A., 1953. Dendritic organization in the neurons of the visual and motor cortices of the cat. J. Anat. 87, 387–406.
Simons, J.S., Garrison, J.R., Johnson, M.K., 2017. Brain mechanisms of reality monitoring. Trends Cogn. Sci. 21, 462–473. https://doi.org/10.1016/j.tics.2017.03.012.
Sonnenschein, S.F., Grace, A.A., 2020. Insights on current and novel antipsychotic mechanisms from the MAM model of schizophrenia. Neuropharmacology 163, 107632. https://doi.org/10.1016/j.neuropharm.2019.05.009.
Steullet, P., Cabungcal, J.-H., Coyle, J., Didriksen, M., Gill, K., Grace, A.A., Hensch, T.K., LaMantia, A.-S., Lindemann, L., Maynard, T.M., Meyer, U., Morishita, H., O'Donnell, P., Puhl, M., Cuenod, M., Do, K.Q., 2017. Oxidative stress-driven parvalbumin interneuron impairment as a common mechanism in models of schizophrenia. Mol. Psychiatry 22, 936–943. https://doi.org/10.1038/mp.2017.47.
Tendilla-Beltrán, H., Arroyo-García, L.E., Diaz, A., Camacho-Abrego, I., de la Cruz, F., Rodríguez-Moreno, A., Flores, G., 2016. The effects of amphetamine exposure on juvenile rats on the neuronal morphology of the limbic system at prepubertal, pubertal and postpubertal ages. J. Chem. Neuroanat. 77, 68–77. https://doi.org/10.1016/j.jchemneu.2016.05.004.
Tendilla-Beltrán, H., Antonio Vázquez-Roque, R., Judith Vázquez-Hernández, A., Garcés-Ramírez, L., Flores, G., 2019a. Exploring the dendritic spine pathology in a schizophrenia-related neurodevelopmental animal model. Neuroscience 396, 36–45. https://doi.org/10.1016/j.neuroscience.2018.11.006.
Tendilla-Beltrán, Hiram, Meneses-Prado, S., Vázquez-Roque, R.A., Tapia-Rodríguez, M., Vázquez-Hernández, A.J., Coatl-Cuaya, H., Martín-Hernández, D., MacDowell, K.S., Garcés-Ramírez, L., Leza, J.C., Flores, G., 2019b. Risperidone ameliorates prefrontal cortex neural atrophy and Oxidative/Nitrosative stress in brain and peripheral blood of rats with neonatal ventral hippocampus lesion. J. Neurosci. 39, 8584–8599. https://doi.org/10.1523/JNEUROSCI.1249-19.2019.
Tendilla-Beltrán, H., del Sanchez-Islas, N., C. M., Marina-Ramos, 2021. The prefrontal cortex as a target for atypical antipsychotics in schizophrenia, lessons of neurodevelopmental animal models. Prog. Neurobiol. 199, 101967 https://doi.org/10.1016/j.pneurobio.2020.101967.
Tseng, K.Y., Chambers, R.A., Lipska, B.K., 2009. The neonatal ventral hippocampal lesion as a heuristic neurodevelopmental model of schizophrenia. Behav. Brain Res. 204, 295–305. https://doi.org/10.1016/j.bbr.2008.11.039.
Vázquez-Roque, R.A., Ramos, B., Tecuatl, C., Juárez, I., Adame, A., de la Cruz, F., Zamudio, S., Mena, R., Rockenstein, E., Masliah, E., Flores, G., 2012. Chronic administration of the neurotrophic agent cerebrolysin ameliorates the behavioral and morphological changes induced by neonatal ventral hippocampus lesion in a rat model of schizophrenia. J. Neurosci. Res. 90, 288–306. https://doi.org/10.1002/jnr.22753.
Vázquez-Roque, R.A., Ubhi, K., Masliah, E., Flores, G., 2014. Chronic cerebrolysin administration attenuates neuronal abnormalities in the basolateral amygdala induced by neonatal ventral hippocampus lesion in the rat. Synapse 68, 31–38. https://doi.org/10.1002/syn.21718.
Winner, B., Desplats, P., Hagl, C., Klucken, J., Aigner, R., Ploetz, S., Laemke, J., Karl, A., Aigner, L., Masliah, E., Buerger, E., Winkler, J., 2009. Dopamine receptor activation promotes adult neurogenesis in an acute parkinson model. Exp. Neurol. 219, 543–552. https://doi.org/10.1016/j.expneurol.2009.07.013.